Physics-Based Simulator for NEO Exploration Analysis & Simulation

J. (Bob) Balaram [*], J. Cameron [*], A. Jain [*], H. Kline [†], C. Lim [*], H. Mazhar [‡], S. Myint [*], H. Nayar [*], R. Patton [§], M. Pomerantz [*], M. Quadrelli [*], P. Shakkotai [¶], K.Tso [*]

Jet Propulsion Laboratory, California Institute of Technology, Pasadena, CA, 91109

As part of the Space Exploration Analysis and Simulation (SEAS) task, the National Aeronautics and Space Administration (NASA) is using physics-based simulations at NASAs Jet Propulsion Laboratory (JPL) to explore potential surface and near-surface mission operations at Near Earth Objects (NEOs). The simulator is under development at JPL and can be used to provide detailed analysis of various surface and near-surface NEO robotic and human exploration concepts. In this paper we describe the SEAS simulator and provide examples of recent mission systems and operations concepts investigated using the simulation. We also present related analysis work and tools developed for both the SEAS task as well as general modeling, analysis and simulation capabilites for asteroid/small-body objects.

The SEAS simulator incorporates high-fidelity models of the NEO environment including its irregular geometry, the gravity field, and the effect of perturbing forces such as other body gravity fields and solar pressure. A local regolith model consisting of many individual irregular particles interacting through friction and cohesive forces can be used to model the details of contact events at or below the NEO surface. The NEO orbit is propagated from planetary ephemerides data and the option is available to model its rotation using either a kinematic or dynamics model. The spacecraft trajectory is propagated in the low-gravity field of the NEO and the simulation is capable of providing collision and line-of-sight information between the spacecraft, NEO and other objects. Representative NEO models based upon the Itokawa and Eros NEOs are currently in use within the simulation and a Phobos model is also under development. Spacecraft and surface assets at the NEO are modeled with full multi-body dynamics and include models for spacecraft devices such as thrusters, reaction wheels, Inertial Measurement Units (IMUs), star-trackers, tethers and anchors. Illumination from the sun is modeled to allow synthesis of images from surface viewing navigation cameras. Standard spacecraft Guidance, Navigation and Control (GNC) functions are incorporated into the simulation to provide attitude and position control. This NEO simulation is based upon the DSENDS spacecraft modeling tool available at JPL that has been previously used on such missions as the Mars Phoenix Lander. Studies being conducted with this simulator in the NEO context include spacecraft-mounted arms performing contact and surface sampling activitites, a surface hopping robots landing interactions with the surface, iterative guidance laws for surface hopping mobility, regular and irregular orbits, station-keeping at various distances and periods, visualization of the surface and near-surface gravity fields, approach guidance simulation, tethered free-flying operations, evolution of dust plume/ejecta arising from surface operations, and anchoring of surface assets.

[*]JPL Autonomous Systems Division, Mobility and Robotics Section; 4800 Oak Grove Drive, Pasadena, California 91109
[†]Rensselaer Polytechnic Institute, Troy, New York.
[‡]University of Wisconsin, Madision, Wisconsin.
[§]Stanford University, Palo Alto, California
[¶]JPL Mechanical Systems Division; 4800 Oak Grove Drive, Pasadena, California 91109

I. Introduction

The SEAS task at JPL performs modeling, simulation and visualization of asteroid and small planetary body missions. SEAS develops high-fidelity models of the environment, deployed systems and the interaction between them under realistic operational scenarios. The objective of SEAS is to provide engineering data from physics-based analysis and simulations to NASA mission designers and planners. We expect these efforts to continue to answer critical questions about feasibility, resource requirements, and system or component performance during planned mission operations. Examples of such questions include:

System Architecture: What are the mission and system elements needed for the mission e.g. a probe operating separately from a standoff spacecraft or an integrated lander. What anchoring concept would allow for in-situ implantation of an instrument on the surface ?

Mission Architecture: What should the duration of the mapping phase be in order to characterize the surface ? What is the strategy for using Solar Electric Propulsion (SEP) during NEO operations ? What strategy should be employed to provide a robust sampling capability ?

Guidance, Navigation and Control: What combination of flight-like algorithms, software and avionics succeeds in achieving mission success with acceptable risk ? What are the attitude control implications (e.g. maximum attitude rates, deadbands, overturning moments) resulting from forces arising from the transition of a complex multi-body spacecraft and sampling arm/mast system from free-flight to contact onto a granular surface ? What are the dynamics of a tether system used to secure an instrument and what level of tether tension control needs to be provided ?

Operations: What are implication on communications and lighting arising from the irregular shape of the NEO ? What are the visibility and operational implications arising from material disturbed and ejected from the surface ?

II. NEO Modeling and Analysis

A. Integrated Model

The analysis capabilities within the SEAS system is built upon an integrated set of physics-based models as illustrated in Figure 1. The block diagram shows each element of the integrated model of spacecraft and end-effector dynamics, including models for the planning function, where the spacecraft trajectory and attitude are specified; the vehicle attitude and orbital dynamics; the vehicle GN&C functions, including orbital and attitude estimator and navigation filters; the deployable manipulator dynamics and its associated hinge actuation; and the end-effector, anchoring, or in-situ sampling device dynamics and actuation. Environmental models include the NEO shape, orbital dynamics, and polyhedral gravity models; and the multi-scale properties of the surface regolith which governs the interaction of the end-effector, anchoring, or in-situ sampling device with the surface. In addition, mission considerations such as the communication geometry, power draw, and scene lighting are also part of the integrated analysis capability.

Consider the example of a sample-collection scenario, where the block diagram would include feedback loops to the spacecraft controller from the hinge states of a deployed robotic manipulator, the end effector states, and the amount of mass collected, assuming all these states are known. If not known, they can possibly be estimated. The reason for including these additional functions is that sensing these states are all possibilities in a scenario where an algorithm is needed to monitor the duration of the sample event (dwell time), and a change in each one of these states can be used as a trigger to terminate the event. For instance, monitoring the flow of collected mass via a photocell will signal that indeed exogenous matter has entered the spacecraft system, and the event "collect sample" can now be terminated. A change of relative attitude of the end effector or boom angle (or hinge angle) with respect to the spacecraft attitude (as measured with respect to the surface plane) will indicate that the end effector has indeed contacted the ground.

B. System and Mission Analysis Process

The analysis process within SEAS is shown in Figure 2. The various elements include:

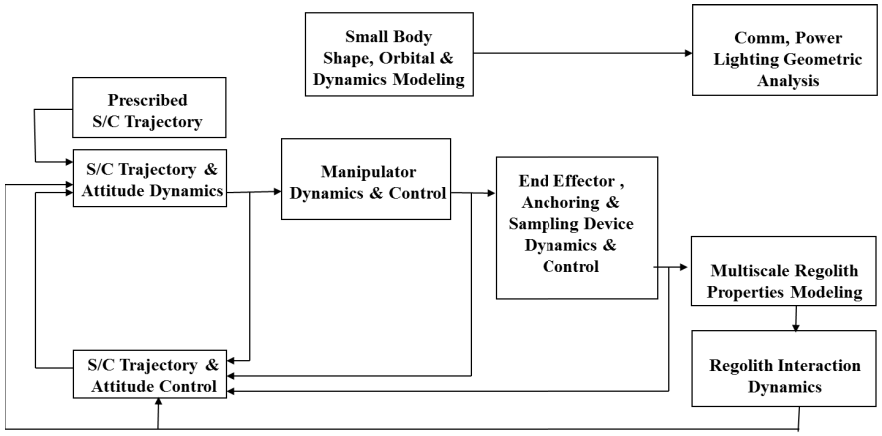

Figure 1. Integrated physics based models

- A set of computation tools provide the foundation of the analysis. These include physics engines for ephemerides, kinematics, spacecraft, manipulators & target body dynamics, terrain shape, regolith granular materials, lighting, scene generation, and line-of-sight geometry. Additional support software such as optimizers and tools for parametric sweeps and Monte-Carlo analysis allow comprehensive data analysis. The computational platforms to execute the software rely on Linux clusters as well GPU/CUDA code accelerators.

- Data generation from simulations provides quantitative metrics that are functions of system state or state history. In addition, the data generation process supports the determination of the performance as a function of parameters in the system. Examples of performance metrics include trajectory times, activity time-lines, delta-V budgets, scene visibility/lighting, power draw and energy needs, site reachability from orbit, and system thermal and radiation loads. Risk related metrics include probability of success/failure and uncertainty quantification through Monte-Carlo simulations as well as direct probability density function propagations.

- Analysis Products which allow for the communication of the results such as reports, 3-dimensional visualization, performance maps and contours, web-accessible query engines that can provide users and user software tools with data, and browsers that allow visualization of high-dimensional trade spaces associated with the system and mission design.

For the NEO scenarios, one can consider the specific analysis that needs to be performed as a function of disciple domain and the mission phase. In the table the various discipline domans (e.g. GNC) are organized along the rows and the various mission phases are organized by the columns.

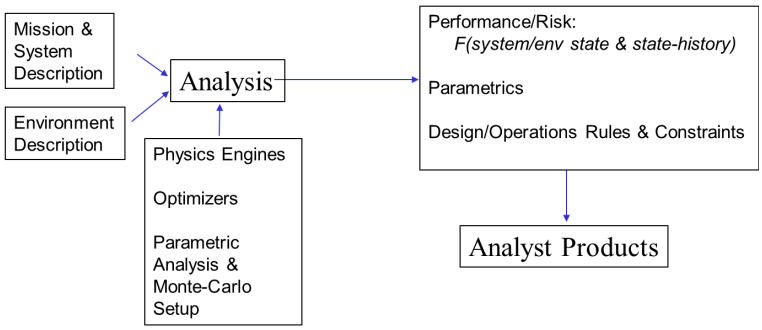

Figure 2. Scenario analysis process

Domain/Phases	Approach/Proximity	Contact Transition	On-Surface	Sub-Surface
Guidance & Planning	Mapping orbits, Approach trajectory & turns; Station keeping; Collision free paths	Impact & Departure profiles; Impressed forces;	Tether tension profiles; Impressed forces	Sampling, digging command profiles
Navigation & Estimation	Landmark-based positions, terrain distances/clearances	Landing state	Anchor, tether states	Sampling, digging states
Sequencing & Control	Reaction-Wheel & Thruster-based attitude and delta-V control; Low-Thrust thruster control	Landing leg, probe, arm force interaction control	Manipulator control; tether tension control; Anchor deployment	End-Effector, Scoop
Sensing & Perception	Camera & Lidar sensing	Dust obscuration	End-Effector forces, anchor tension	End-effector forces; Drill, coring forces
Power & Energy	Solar eclipsing		Actuator power	Drilling & sampling energies

III. SEAS Simulator

The SEAS simulator is a product of the Dynamics and Real-Time Simulation Laboratory (DARTS Lab) at JPL. The DARTS Lab has been developing high-performance space vehicle simulations for a variety of NASA cruise/orbiter, atmospheric entry/descent/landing, surface rover operations, and formation flying missions. The lab's multi-mission simulations are based upon the Dshell multi-mission simulation framework for integrating reusable hardware and environmental models with the Darts dynamics models to develop high-fidelity spacecraft engineering simulations. The Dshell-based simulations can be used as stand-alone simulations, can be embedded within Matlab/Simulink CAE environments, can be run in closed-loop with flight software, and can also be used within real-time hardware-in-the-loop testbeds. Dshell simulations have been used by several NASA missions including Cassini, Mars Pathfinder, Deep Space 1, SIM, Starlight etc. for their real-time and non-realtime testbed simulation needs. The Dshell framework has been adapted for specific mission domains and is the basis for the ROAMS (Rover Analysis Modeling & Simulation) planetary rover simulator. In recent planetary missions, JPL has developed a Dshell-based tool called DSENDS (Dynamics Simulator for Entry, Descent and Surface landing) to assist in planning entry, descent, and landing (EDL) operations. It has been used for several missions including the Mars Phoenix and upcoming MSL missions. Both ROAMS and DSENDS build upon lower level infrastructural tools such as

the SimScape[1] terrain modeling layer and the Dspace[2] real-time graphics visualization tool.

SEAS builds on the Dshell-based Lunar Surface Operations Simulator (LSOS) package[3,4,5] for modeling, simulating and visualizing surface operations on the moon. LSOS, in turn, derives its heritage from the ROAMS, DSENDS, SimScape, Dshell and DARTS dynamics simulation packages[6,7,8,9,10,1] developed at JPL. LSOS was used to determine performance of surface systems and to analyze and optimize lunar mission plans. High-fidelity models of the lunar surface and the physical and operational behavior of systems deployed on the surface were developed and simulated in LSOS. Results from the analysis and simulations performed with LSOS include energy needed to perform specific traverses, energy generated by solar panels in specified operational scenarios, communication to other ground and orbiting assets, life support resource usage, thermal dynamics and radiation modeling. Last year the Missions Operations Division (MOD) at NASA's Johnson Space Center (JSC) and the DARTS Lab team at JPL jointly worked on extending the Dshell/DSENDS framework for use in a wide range of MOD missions. The DARTS Lab group teamed with MOD team from JSC to formulate a new generation of Dshell/DSENDS called DshellCommon that is more flexible and can be applied to a wide range of missions such as ascent, rendezvous, orbital operations, entry, descent, and landing. DshellCommon provides simulation tools at several levels. An end-user can execute pre-generated scripts to easily do mission analysis. A more experienced user can use a powerful library of components to construct their own runtime scripts to construct new or modified simulations. More advances users can create their own components to model new types of hardware or mission-related functionality. SEAS inherits all these capabilities and extends them for operations near and on small bodies.

A. Functional Capabilities

We provide an overview of the key functional capabilities of the DSENDS simulator that are especially relevant to NEO modeling, analysis and simulation. Many of the functions are encapsulated into modular, reusable models organized into libraries, as well as various engines and middleware framework elements.

1. Vehicle Dynamics & Kinematics

These include models for lander and ascent vehicles, the Multi-Mission Space Exploration Vehicle (MMSEV), viscoelastic lines/tethers, reel-out and deployment devices, and anchors. Data-driven models of multiple articulated bodies, their separation, center-of-mass shifts resulting from fuel depletion, and fuel slosh are available for use. The bodies in the simulation can be flexible thereby allowing the capture of both rigid and flexible modes in the system dynamics. In addition to the kinematics of articulation elements, the simulator can also model collisions and perform coordinate frame and line-of-sight computations.

2. Device Models

The include sensor models for Inertial Measurement Units (IMUs), altimeters, velocimeters, descent camera, and visual landmark detection and recognition. The library includes actuation models for throttled descent engines and thruster, reaction wheels, and motorized gear elements that actuate gimbals and robotic manipulators. Also included are ancillary models such as those for battery power storage, solar panels and consumables within the spacecraft.

3. Space Environment

These include gravity models in the form of spherical harmonics as well as polyhedral gravity models for the irregular target body shapes of NEOs. In addition NEO ephemerides is modeled using Spice kernels. Radiation models for monitor astronaut dosage are also available.

4. Terrain Shape

Terrain shape can be represented in SimScape on a spherical coordinates grid (suitable for planetary bodies), as Digital Elevation Maps (DEMs), or as general meshes (suitable for the irregular shapes of NEO objects). The data for the shape models can be of arbitrary size as utilities within SimScape terrain modeling layer provides for rapid dynamic paging of data into memory.

5. *Scene Geometry*

Many of the simulations involve geometry of both the terrain and the vehicle. A framework element within SEAS called DScene manages the various geometry data. This is used to pipe geometry data into visualization, scene analysis and collision detection libraries.

- **Visualization.** The visualization library within the simulation is called Dspace.[2] It is built on top of the OGRE open source rendering engine. Dspace provides the ability to render a 3D scene graph in real time. It has features such as GPU-based continuous level of detail for terrains, textured-based shadows, and a thread-safe Python and C++ API. Dspace supports multiple camera views that are used to display various points of view of the spacecraft and environment during a simulation. Because camera position, pointing and field of view angle can be precisely controlled by the simulation, scenes can be rendered from the point of view of all spacecraft-mounted navigation and science cameras. When running in closed-loop mode with simulated or actual on-board navigation or pointing control software, Dpace can render a scene from the point of view of a spacecraft mounted camera and feed that rendered image back to the control software for processing and analysis. Control software changes to the simulated spacecrafts attitude will be reflected in later Dspace camera point of view rendered images. In this control software-in-the-loop mode, Dspace can render camera point of view images as spacecraft position and attitude is continuously modified by the control software.

- **Scene Analysis.** To successfully navigate a spacecraft near the surface of an irregularly shaped NEO, it is critical to understand important mission constraints, such as the shape of local horizon, when the spacecraft will enter shadow, when the NEO will occult the spacecrafts link to Earth, and when multiple spacecraft in the NEO vicinity can communicate with each other. Current analytic methods for characterizing irregular body shape and rotation and with respect to spacecraft are difficult to implement and computationally very expensive. Alternate techniques utilizing the graphics hardware and engines have been adapted for this purpose. For example, during a NEO simulation, using a technique similar to that used in the LSOS simulator, images of the suitably monochrome textured target NEO would be rendered from the point of view of a nearby spacecraft against a black background. Examining the image pixel boundary between the known NEO texture color and the background allows the determination of the achieved horizon. The set of detected horizon pixels, along with their inertial coordinates, camera location and pointing information, is returned to the simulation for further processing. Mission designers and planners can use this shape information to plan spacecraft orbits, trajectories and communication opportunities. Another example of such a scene analysis technique, also successfully used in the LSOS simulator, is to render an emissive colored solar panel model from the vantage point of the sun-direction vector. The number of emissive pixels rendered in the scene directly correlates to the illumination on the panel and takes into account both self-shadowing and light obstructed by the NEO or other assets.

- **Collission Detection.** BulletScene is the collision detection library within the simulation and is built on an open source library called Bullet. The collision detection facility is used for analyzing trajectories of the spacecraft or robot arm for collisions with other physical objects. The capability can also be used to find ray intersections with the objects in the scene. For example, point-to-point line-of-sight can be evaluated using collission detection between a line segment joining the points of interest and the NEO shape model.

6. *Regolith*

The SEAS simulations normally use a fast multi-body simulation based on the DARTS dynamics engine for propagating the spacecraft state when in free-flight about the NEO. During contact with the NEO a spring-damper model can be used with multi-body dynamics. However, for more accurate simulations, where the interaction forces emerge *ab-initio* from the detailed interaction of particles in the regolith media, a granular material simulation is used.

SEAS models for granular material physics are compuationally intensive and are therefore implemented using GPU/CUDA techniques. Very few GPU projects are concerned with the dynamics of multibody systems, the two most significant being the Havok and the NVIDIA PhysX engines. Both are commercial and proprietary libraries used in the video-game industry and their algorithmic details are not public. Typically,

these physics engines trade precision for efficiency as the priority is in speed rather than accuracy. In this context, the goal of our effort was to somewhat de-emphasize the efficiency attribute and instead implement an open source, general-purpose physics-based GPU solver for multibody dynamics backed by convergence results that guarantee the accuracy of the numerical solution.

Unlike the so-called penalty or regularization methods, where the frictional interaction can be represented by a collection of stiff springs combined with damping elements that act at the interface of the two bodies, the approach embraced here draws on time-stepping procedures producing weak solutions of the differential variational inequality (DVI) problem, which describes the time evolution of rigid bodies with impact, contact, friction, and bilateral constraints. Recent approaches based on time-stepping schemes have included both acceleration-force linear complementarity problem (LCP) approaches and velocity-impulse, LCP-based time-stepping methods. The LCPs, obtained as a result of the introduction of inequalities accounting for non-penetration conditions in time-stepping schemes, coupled with a polyhedral approximation of the friction cone, must be solved at each time step in order to determine the system state configuration as well as the Lagrange multipliers representing the reaction forces. If the simulation entails a large number of contacts and rigid bodies, as is the case for granular materials, the computational burden of classical LCP solvers can become significant. Indeed, a well-known class of numerical methods for LCPs based on simplex methods, also known as direct or pivoting methods, may exhibit exponential worst-case complexity. Moreover, the three-dimensional Coulomb friction case leads to a nonlinear complementarity problem (NCP). The use of a polyhedral approximation to transform the NCP into an LCP introduces unwanted anisotropy in friction cones and significantly augments the size of the numerical problem.

In order to circumvent the limitations imposed by the use of classical LCP solvers and the limited accuracy associated with polyhedral approximations of the friction cone, a parallel fixed-point iteration method with projection on a convex set has been developed. The method is based on a time-stepping formulation that solves at every step a cone-constrained quadratic optimization problem. The time-stepping scheme has been proved to converge in a measure differential inclusion sense to the solution of the original continuous-time DVI. Using this method a GPU based simulation capability was implemented in the open source Physics Engine: Chrono::Engine.

While these advances allow for fast granular material simulations, the time-scales of a DARTS multi-body dynamics engine using an empirical spring-damper model of regolith interaction and the Chrono::Engine particle simulation still differ by many orders of magnitude. To establish and end-to-end simulation capability, a simulation state handoff between the two simulations is used. The DARTS engine is used for state propagation "in the large" i.e. over the entire spatial/temporal extent of the NEO simulation, and the Chrono::Engine simulation is used to implement a "sandbox" in the vicinity of the anticipated short-duration regolith interaction. State information relevant to each simulationi is exchanged using an XmlRPC protocol to allow seamless propagation of the system state. The role of the "sandbox" within the NEO simulation together with a visualization of its internal contact state is shown in Figure 3. Here the contact force intensity is encoded into red colored zones whose geometric extent allows visualization and correlation with validation experiments.

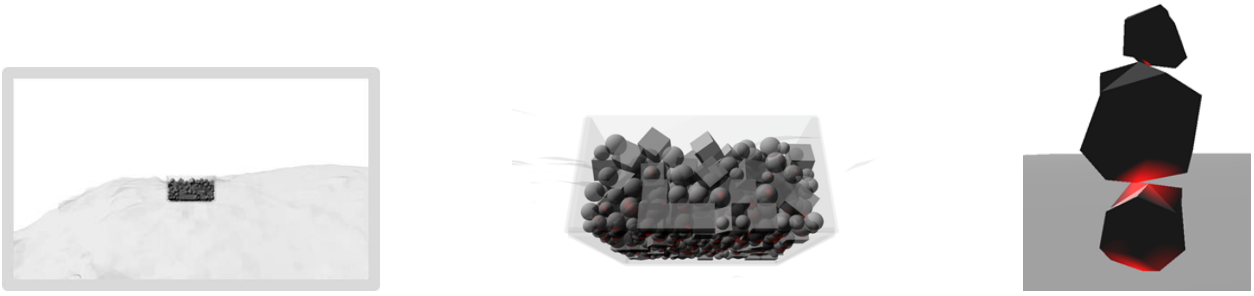

(a) NEO Scale Simulation

(b) Regolith Sandbox

(c) Regolith State Visualization

Figure 3. Regolith sandbox within main simulation

7. *Simulation Facilities*

Python is uses as both a scripting language to set-up simulations as well as an interpreter interface to the underlying implementation of the simulation code in C++ and C. Legacy and third-party code in Fortran is also supported. User scripts can call out to Matlab for specialized computations and the whole simulation can be used within Simulink. For embedded use, a purely C++/C system can be used as a library without the need for the Python system.

The simulator has facilities to checkpoint the simulation at any time, generation of context dependent data logs., real-time plotting, GUI-based simulation introspection, and 3-d graphics visualization. Facilities are also available for automated Monte-Carlo & Parametric simulation setup with user-specifiable variate generation from a variety of probabilistic distributions. System performance impact resulting from computational issues can also be examined by allowing for computational cycle time budgets of the eventual target computer to be emulated. A large set of GNC stub code is available to allow the rapid construction of functional end-to-end spacecraft and robotic systems.

A data logging facility, called DLogger, has been developed for post-simulation analysis and replay. When logging is turned on, DLogger automatically logs all the objects in the 3D scene and the data generated in each simulation step. These data enable the replaying of the complete simulation as well as analyzing the simulation results. Several plugin tools have been developed to facilitate the visualization and analysis of these data. These include a *strip-chart* plugin that enables the plotting of simulation data with the selection of data columns, a *play-back* plugin that enables the 3-d replay of the simulation viewed from different viewpoints and replayed at different speeds, and a *movie-making* plugin that allows the selection of keyframes, transitions, and speeds to create movies in different video formats. DLogger uses the HDF5(*) technology for storing the data. HDF5 provides a versatile data model that accommodates the complex data objects in the 3D scene, as well as efficient storage for the high-volume simulation data of a wide range of data types. HDF5 also provides high-performance random access in retrieving the data and optimization in storage space.

8. *Simulation Data*

Models developed in SEAS are generalized through the use of parameters that specify particular instances of the model. For example, the mechanical interaction properties of soil and regolith in SEAS is parameterized by its cohesion, density and internal friction. A particular instance of sand, clay, or other type of soil can then be created for a specific simulation using the appropriate parameters. Model parameters for specific applications are determined from the research literature or through experiments conducted in testbeds. Data obtained from experiments are crucial in determining parameter values to correctly model the complex dynamics behavior of systems. For SEAS this includes experimentally determining the appropriate parameter values to use in manipulator-soil contact dynamics and standoff arm anchoring. Testbeds can also serve as a validation and verification tool by corroborating simulation results against experimental results.

B. NEO Environment

Some observations can be made about the NEO environment by comparing it that of the Moon (Table **??**. We then discuss some of these differences as they impact the modeling of the phenomena within SEAS.

Phenomena	Moon	NEO
Gravity	Higher order harmonics from mascons at the milliGal level	Polyhedral models
Surface Acceleration	Same as gravity accelerations	Order of magnitude variations because of rotation rate
Orbital Stability	Long term drift due to mascons	Mix of stable and unstable orbit families
Target body orbital period	$\approx$ 30 day period	Hours
Porosity	Small	$30 - 50\%$
Morphology	Planet-like	Rubble pile
Regolith mechanical properties	Friction dominated (like sand/rocks)	Cohesion dominated (like large-scale flour)
Noteworthy surface features	Rocks, craters	Rocks; electro-statically generated dust ponds; large-scale cohesively bound structures

1. *Gravity Models*

The highly irregular shapes of many asteroid and other small bodies lead to unique modeling and dynamics challenges. In contrast to the gravitational fields of spherical and ellipsoidal bodies, those produced by near earth objects are frequently much more complex. The gravitational fields of these irregular bodies exhibit high levels of variation at both the surface and locations near the bodies. In addition, these gravitational fields are often orders of magnitude weaker than Earths. Figure 4 illustrates both the low magnitude and substantial variation of the modeled gravitational acceleration at the surface of the asteroid Itokawa.

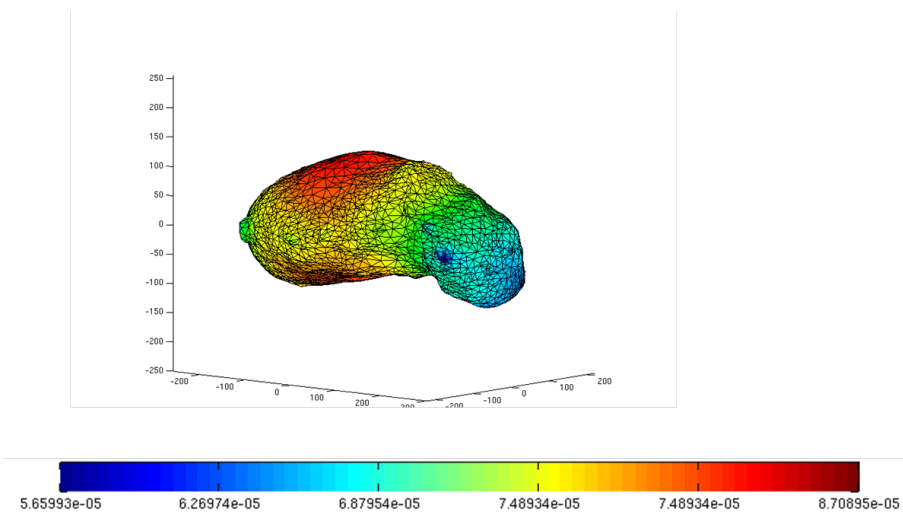

Figure 4. Surface acceleration on Itokawa asteroid

Figure 5 provides a vector field representation of the gravitational acceleration around 433 Eros. Variations can be observed corresponding to the irregular geometry of the asteroid.

To observe the effects of gravitational irregularity, several simulations of a small mass orbiting about 433 Eros were performed (see Figure **??**). A stable behavior is exhibited by a mass orbiting about the short dimension of 433 Eros. When an attempt was made to orbit the mass about the long axis of the asteroid, instability was observed. These simulations highlight the influence of gravitational variations near small bodies on spacecraft dynamics.

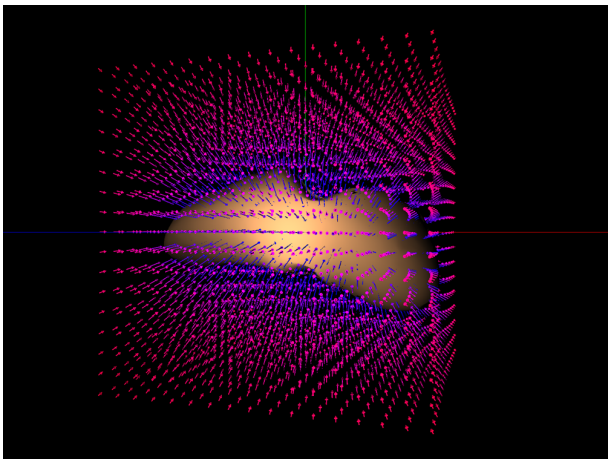

Figure 5. Gravity vector field on Eros asteroid

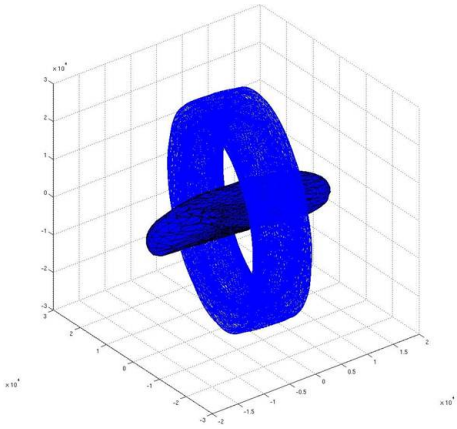

(a) Stable Orbit Bundle

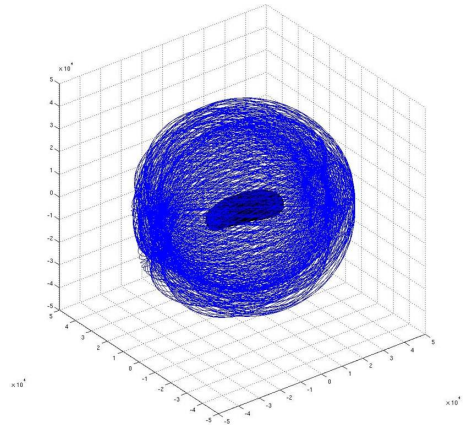

(b) Unstable Orbit Bundle

Figure 6. Stable and unstable orbits.

In addition to exhibiting irregular shapes, the gravitational fields produced by small bodies often have milli-G or micro-G order magnitudes as shown in the Table. As a result, escape velocities from these bodies are exceptionally low and must be carefully considered when maneuvering landers or spacecraft. Another consequence of these low gravitational magnitudes is that the rotational period of the small body may impact the movement or trajectory of a spacecraft or lander. It may be possible to take advantage of this behavior to aid in movement between surface locations on a small body. This could potentially be achieved by applying an impulse to the lander such that it hops away from the surface without an orbital velocity component while the small body continues to rotate. This maneuver would lead to a change in position when gravity pulls the lander back to the surface. As the topics examined illustrate, it is necessary to understand the impacts of both small gravitational magnitudes and irregular gravitational field shapes to ensure successful spacecraft interactions with small bodies.

Gravity Order-of-Magnitude	**Total Surface Acceleration**	**Body**
1 G	1 G	Earth
0.1 G	0.17 G	Moon
1 milli-G	0.2 to 0.6 milli-G	Eros (18 km)
10 micro-G	6-9 micro-G	Itokawa (0.18 km)

2. Regolith Models

Behavior of the regolith is likely governed by cohesion and surface adhesion effects that dominate particle interactions at small scales through van der Waals forces.[11] Electrostatic forces are are generally negligible except near terminator crossings where it can lead to significant dust transport. The micro-gravity and solar radiation dominate system behavior prior to soil engagement or penetration.

At very low gravity and vacuum conditions the biggest unknown is the material strength of the surface material.[12] Neither the Deep Impact mission nor other comet observations have provided firm data on the strength of cometary material. Theoretical considerations and laboratory measurements for weakly bound aggregates and the few observational constraints available for comets and cometary meteoroids lead to estimates of the quasi-static tensile (or shear) strength of cometary material in the dm- to m-range as of the order of 1 kPa, while the compressive strength is estimated to be of the order of 10 kPa.

Cohesion, tensile, shear and compressive strength: While for brittle materials, tensile strength is generally less than the shear strength, compressive strength is about one order of magnitude higher than tensile strength. In the case of soft landing compressive strength is the relevant parameter. Shear, tensile and compressive strength are indicated by σ_s, σ_t, $sigma_c$, respectively.

Dynamic and quasi-static strength: During impacts, due to very high strain rates, the dynamic strength is typically higher than the quasi-static strength. It is known that the strength increases with strain-rate resulting in values about an order of magnitude higher (or even more) than the quasi-static strength for the same material. Generally the tensile strength σ_t is proportional to a power b of the strain rate $\dot{\epsilon}$ with a power law exponent typically around 1/4 to 1/3, depending on the material.

Size dependence: Different theories indicate that the strength decreases with increasing sized according to $\propto d^q$ where the exponent q is ≈ 0.5 (fractal aggregate with fractal dimension $D = 2.5$ of ice). Thus, if extrapolated from typical lander (0.1 m), or impactor (1 m) to typical comet (1 to 10 km) scales, the size effect alone would produce a factor of 100 in the apparent strengths. This is in line with the observation that comets can often be described as essentially strength-less bodies (large cometesimal, rubble pile, swarm models) globally, while locally a significant material strength is to be expected.

Breakup of Comets, Topography Observations Tidal disruption of comets indicate low global tensile strengths in the order of 10010,000 Pa. For example, the break-up of Shoemaker-Levy 9 during its perijove in 1992 set a rough upper limit of the tensile strength (on global/km scales!) of 100 Pa. The tensile strength of sun-grazing comets has been estimated as 10 kPa with some uncertainty due to thermal stresses. Images by Stardust from comet 81P/Wild-2 showed that the cometary surface must have a finite strength on short scales ($< 100m$) to support the observed topographic features; because of the small gravity, some 10 Pa might suffice. Otherwise, only lower bounds on the tensile strengths are available in the order of $1 \ldots 100Pa$.

Breakup of Meteoroids Another source of information about possible strength values of cometary surfaces on mm-dm scales stems from the analysis of meteoroids associated with certain comets which enter the earth atmosphere at high speeds and finally break-up and create a light flash. Wetherill gives values for tensile strengths of these fireballs ranging from 1 kPa to 1 MPa. More recently, Trigo-Rodrguez and Llorca have studied a broad data base of meteor ablation light curves and arrive at tensile strengths between (400 ± 100 Pa and 40 kPa, clustering around 10 kPa for not too evolved and rather low density $< 1gcm^3$ (if known) cometary meteoroids.

Laboratory Measurements: The small scale (cm) shear and tensile strength of snow in the relevant density range of 300500 kg m3 is of the order of 10100 kPa . The tensile strength of snow is nearly independent on temperature, while the compressive strength shows a remarkable increase with decreasing temperatures. Simulating possible cometary analogue material in the scope of the KOSI experiments, Jessberger and Kotthaus conclude that the small-scale compressive strength of porous mixtures of crystalline ice and dust lies in the range between 30 kPa and 1 MPa with increasing strength for an increasing dust fraction.

Limits Derived from Comet Size and Rotation: Stability against disruption due to rotation yields lower limits of a combination of bulk density and tensile strength. Rotational periods and sizes for many comets are known, but bulk density is not well constrained, so until now this method does not give us a constraint on the strength of comets (e.g., fast rotating and big comet C/Hale-Bopp (1995 O1) could be a strength-less rubble pile with a bulk density as low as $100kg/m^3$ it probably is indeed damaged.

Theoretical Estimates: There are different approaches to describe the tensile strength of powders on the basis of van der Waals interactions, cf. Greenberg et al. or Chokshi et al., the latter model including the elastic deformation of contacting spherical grains. The theoretical tensile strength of fluffy aggregates depends on particle radii, contact areas, packing geometry and typically scales with the bulk density. Greenberg et al. estimate a tensile strength, for interstellar silicate dust/ice material with a density of $280kg/m^3$, of 270 Pa. Sirono and Greenberg derive 300 Pa for the tensile and 6000 Pa for the compressive strength for a medium composed of ice grains linked into chains by intermolecular forces. Kuhrt and Keller derive a theoretical strength of 100 Pa and 100 kPa for grains of 1 mm and 1 m, respectively. Note that 95% of the Deep Impact ejecta dust cross section is represented by particles$r < 1.4\mu m$. From the discussion above the conclusion can be drawn that the cometary surface on meter scales has a reasonable lower limit of the tensile strength of the order of 1 kPa whereas the probable upper limit can be taken as 100 kPa.

3. Verification approaches to regolith simulation

Verification and Validation (V&V) is necessary to make sure the correct equations modeling the physics are correctly implemented in software. Validation of the simulation model with experimental results is also necessary to correctly capture the physics in simulation. While verification can be done at the software level, validation with experiment, especially experiments in micro-gravity, tends to be very costly. Therefore, other approaches for V&V of microgravity physics models need to be sought. Figure 7 shows several snapshots of a GPU-driven multibody dynamics simulation of the Brazil nut segregation problem. This is an exampel of an experiment conducted in the SEAS simulator to verify, at the macro-scale, the granular media physics modeling engine. Soil mechanics experiments have know issues when it comes to testing samples of regolith in 1-g. First, a reproducible preparation of a homogeneous soil sample is difficult to achieve. Second, a characterization of the soil properties in depth is difficult, since static parameters are typically measured at the surface. Third, under 1-g load, according to soil theory, the compressive strength in depth is significantly influenced by overburden terms, i.e. the effective strength/resistance increase with depth. The soil shear stress can be modeled as $\sigma c = c + ptan(\phi f)$ i.e. , the Mohr-Coulomb limit soil bearing capacity theory, where ϕf, is known as the friction angle (or internal-angle-of-friction), p is normal pressure, and the zero normal-stress intercept, c, is known as the cohesion (or cohesive strength, i.e. shear stress at p=0) of the soil. For typical regolith simulant, the cohesion is $\approx 40Pa$ at loosely packed conditions and increases to 10 kPa at 100% relative density. The friction angle also increases monotonically from 25 deg to $\approx 60deg$. The Rosetta Lander design takes advantage of this effect of greatly increased cohesion by local compression of the cometary regolith under the landing pods during landing. Previous relevant regolith modeling work[13,12,14] covers both low-velocity ($\approx 1m/s$) impact of blunt bodies into dust-rich, fluffy cometary materials, as well as high-velocity (10 m/s) impact of sharp projectiles on various types of soil. (Anderson et al). The lower limit of the tensile strength is of the order of 1kPa whereas the probable upper limit can be taken as 100kPa. The lower limit of tensile strength corresponds to a compressive strength of $\sigma c > 7kPa$. This wide range of soil properties must be capture in simulation, which poses a significant challenge.

Validation experiments being considered for further validation of the SEAS regolith models include those that use:

- photo-elastic methods, where stress chains are viewed in cross-polarizers
- pink plastic beads, where the contact between polystyrene ball and pink translucent plastic sheet is observed
- wet beads, where water between glass beads provides cohesive forces
- vertical emplacement tests using penetrator shot by gun
- vertical soil bearing capacity tests using regolith simulant
- neutral density beads floating in water, coated with vaseline or silicon oil.

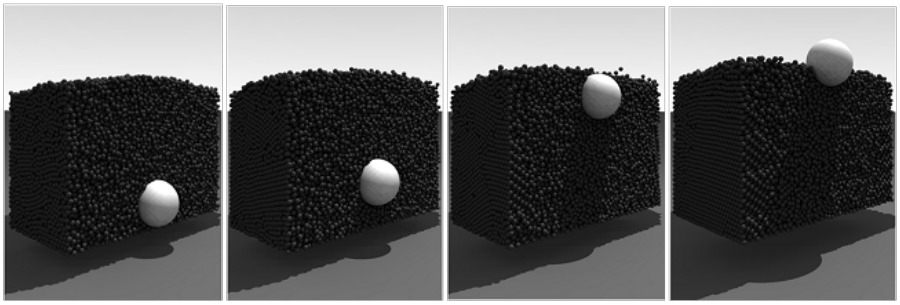

Figure 7. Snapshots of Brazil nut simulation using GPU-driven multibody dynamics modeling

IV. NEO Scenarios

We now describe a number of scenarios that have been simulated in the SEAS system. We also summarize some of the relevant analytical studies conducted at JPL that are related to NEO operations.

A. Approach and Orbit

An examples of a scenario that has been simulated within the SEAS system is **Approach and Orbit** where the spaceraft (Figure **??**) approaches the NEO and establishes a trajectory around the NEO for the purpose of mapping or proximity operations. This trajectory can be a true orbit or it can be in the form of so-called "ping-pong" orbits where the spacecraft performs a delta-V maneuver at end of each trajectory segment, allowing the spacecraft to move back and forth past the NEO, but never establishing a true orbit. In other cases, a pseudo-orbit may need to be established where the spacecraft rotates about the NEO with a desired period of rotation at a desired distance. If the desired period matches the rotation rate of the asteroid then one would have a NEO-stationary pseudo-orbit. Such a trajectory would be useful for sustained observation of a given location on the NEO or for conducting a proximity operations such as probe deployment.

In this example, the Small-Body mass was taken as 542891 kg with a rotation period of 7.6 hrs. The gravity of the central body as well as two perturbing bodies was modeled in the simulation. The disturbance effects of solar pressure were also modeled. A simulation run corresponding to a total sequence time of 20 minutes was generated.

B. Robotic Hopper

Scenarios involving **Surface Mobility** in the low gravity environment of a NEO may involve a robotic hopper. The hopper would launch itself from the surface by means of an actuated foot with the resulting delta-V providing a trajectory that takes the robot to the destination point (shown in green in Figure 9) within an acceptable distance, and with the landing vector in a suitably narrow cone of impact directions i.e. avoiding near horizontal landings. An iterative search using a simulation of the hopper finds the best

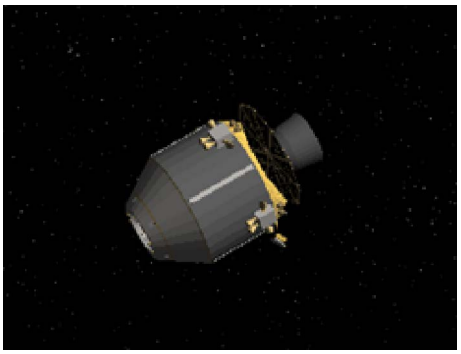

Figure 8. Spacecraft at NEO

hopping delta-V that meets the constraints of the actuator as well as that of landing. Figure 9 also shows the quantities that guide the convergence of the iterative search such as miss distance/angle, and speed.

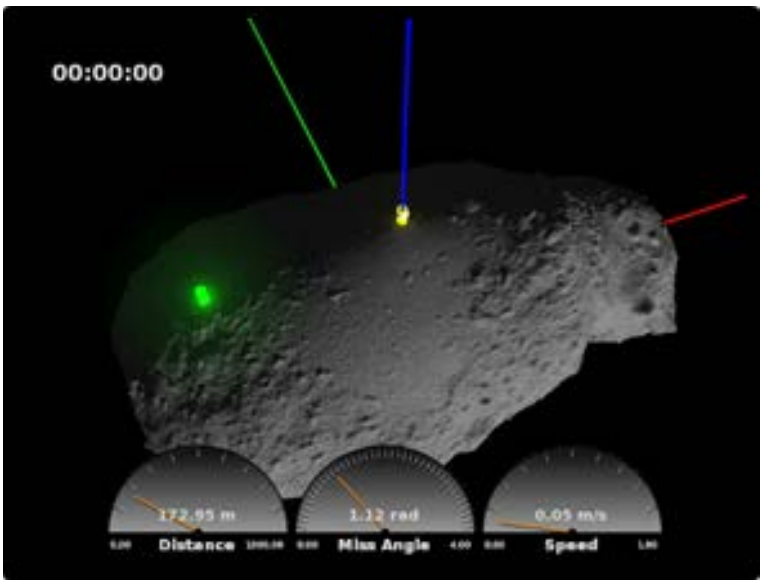

Figure 9. Hopper guidance

Key features include the model of the Itokawa asteroid which has dimensions of (561.5m, 305.6m 243.5m), and an orbit period of 12.13 hrs. The simulation used 3.2 million polygon shape model and a 6000 simplex gravity model for the target body. The orbit for the body was propagated using Spice. The guidance law was designed for a maximum hop velocity of 7.5 cm/sec per axis, and a landing angle constraint of 67.5 deg half cone. The target for the hopping was $\approx 200m$ from the starting location.

C. Surface Ejecta

When the surface of a NEO is disturbed, the low gravity environment requires that **Impact Ejecta** be considered. Such ejecta can be the result of an instrument/device deployment, an anchor/footpad placement, or an astronaut footfall. The dust/ejecta driven up from the surface impacts visibility and the long settling times associated with the NEO implies long settling times. We have simulated ejecta using our dynamics simulation. This involves simulated trajectories of each particle, which we can do in parallel.

An example of our previous ejecta simulation involved simulating ejecta on the Itokawa asteroid. We used a 3.2 million polygonal shape model of Itokawa for doing collision detection and visualization. The polyhedral gravity model we used was based on a lower resolution Itokawa model. We randomized ejecta velocities for 5000 individual particles and ran the dynamics simulation. We also modeled solar light pressure.

This was done using our BulletScene collision detection library to detect when particles were in contact with sun light.

The dust particles are visualized by Dspace as transparent billboard graphical object. Each object accurately moves along the simulated dust trajectory. The position of the graphical objects can be interpolated to smoothly playback the ejecta playback in cases where the simulation step size is large.

Figure 10. Dust and ejecta resulting from surface disturbance

D. MMSEV Spacecraft Control

The Multi-Mission Space Exploration Vehicle (MMSEV) is a vehicle concept for NEO proximity operations. One baseline concept of the MMSEV has the spacecraft assembly with 24 throttled thrusters, 3 reaction wheels, fuel tanks and a number of manipulation arms. The main spacecraft is shown in Figure **??** (without the arms and solar panels) operating in the vicinity of the Itokawa asteroid.

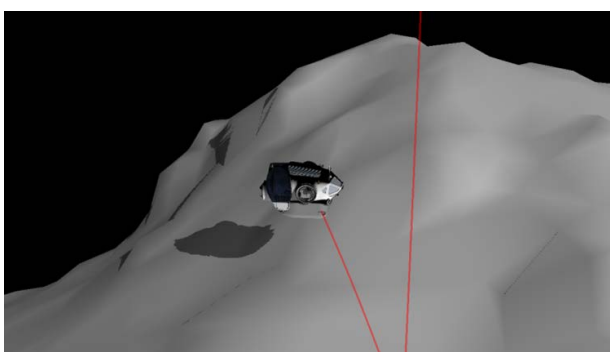

Figure 11. MMSEV vehicle operating near Itokawa

Reaction Wheel (RW) and a thruster Reaction Control System (RCS) are currently simulated in Dshell-Common for spacecraft Guidance, Navigation, and Control. Both RW and RCS control have been simulated with an initial rotation applied, and both are able compensate for the rotation and return to an inertially stationary orientation. The thrusters are also able to return the spacecraft to a given location. The reaction wheels are modeled as bodies in the assembly which are given a prescribed angular velocity in order to provide the required torque. The thrusters in the simulation are throttled thrusters, which vary they apply to the spacecraft assembly based on the needed forces and torques. An example of the attitude history using the RW control is shown in Figure 12, where we see a large attitude error controlled to within deadband

The levels of these thrusters are determined through an iterative control allocation scheme. The abilities of the thrusters to provide forces and moments is composed into a six by n matrix. The pseudo-inverse of this control effectiveness matrix is multiplied by a vector representing the desired control action, producing

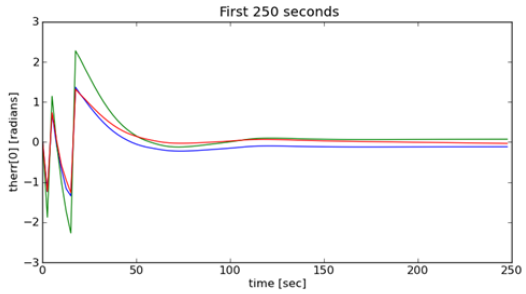

Figure 12. Reaction wheel control

an initial solution which is checked against the maximum levels possible from the thrusters and then iterated to adjust the solution if necessary. An alternative control allocation method can be implemented in the simulation, using the sequential least squares method from QCAT.

Station-keeping about the NEO is currently being studied in simulation. The goal of station-keeping is to keep the space craft in a NEO-synchronous orbit with constant attitude relative to the NEO. This is useful both for near-surface operations where the spacecraft should be kept stationary relative to the surface and for orbits further away from the surface for observation of the asteroid. At a particular radius the force of gravity provides the centripetal acceleration to maintain a circular orbit, but at any other distance fuel is needed to keep the spacecraft at the correct speed. The fuel needed to maintain a stationary orbit about Itokawa has been calculated at several altitudes, using basic rocket equations and disregarding non-uniform gravity, the changing mass of the spacecraft, and fuel needed for attitude adjustments. Preliminary station-keeping results from the simulation using thrusters have been obtained for comparison, although due to differences between these results and the analytical calculations alterations are likely needed for the station keeping algorithm in the simulation.

Five robot arms are mounted on the MMSEV. There are three stand-off arms used to anchor the MMSEV to an asteroid and two manipulator arms to collect samples and perform other science operations. Detail models for the arms were developed at the Johnson Space Center and provided to our SEAS development team at JPL. Dynamic models of these arms along with joint torque motors to actuate the arm have been incorporated into the SEAS modeling environment. Representative arm dynamic parameters are currently being used because the actual parameters are not yet available. Figure 13 shows the port-side standoff and manipulator arms modeled in SEAS.

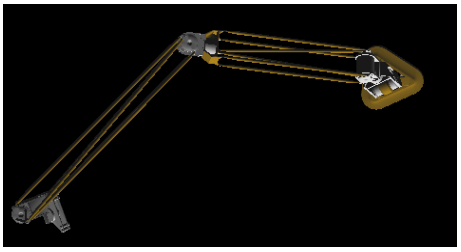

(a) Port-side Standoff Arm

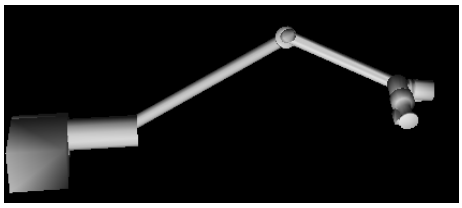

(b) Port-side Manipulator Arm

Figure 13. MMSEV Arms

E. Tethering Near Small Body

In **Tether Operation** scenarios a flexible tether is used to connect the spacecraft and a payload or an astronaut (Figure 14). The deployed tether allows proximity operations without having the main spacecraft in close proximity to the NEO thereby minimizing the operational risks to the spacraft. In the figure an end-mass with a mass equivalent to that of an astronaut is connected to the spacecraft by means of a flexible tether. The flexible tether was modeled as a serial chain of many small links connected together. A 20 m

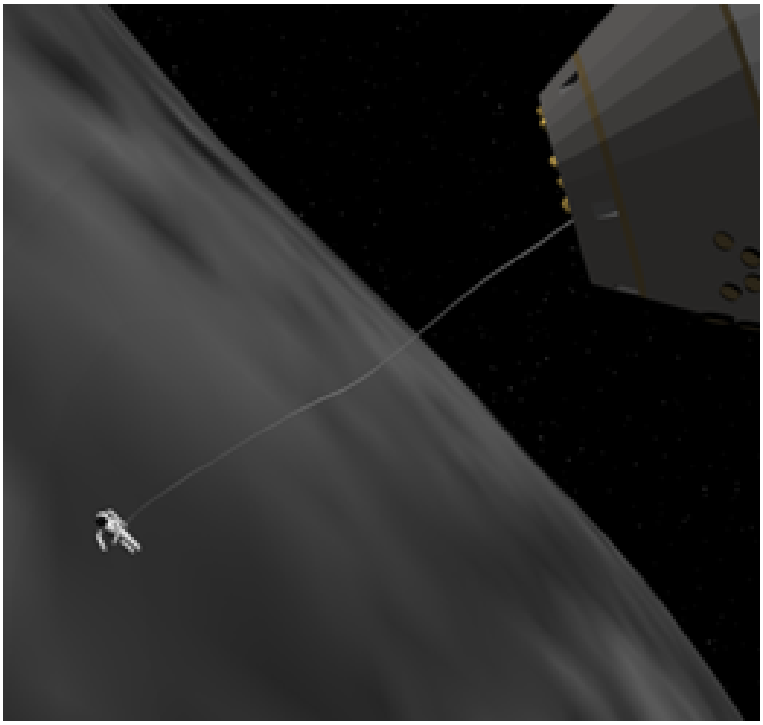

Figure 14. Tether Operation

tether with a density of 1 kg/m was modeld with a stiffness and damping of 0.1 N/rad and 0.1 N sec/rad respectively. The astronaut was modeled as a 200 kg object.

F. Touch-and-Go Sampling

Another example is a **Touch-and-Go Sampling Operation** which involves the spacecraft approaching the NEO using optical navigation and altimetry/velocity sensing. A target-site relative rate nulling i.e. station-keeping is achieved followed by a vertical descent phase. When the spacecraft is sufficient close to the surface, a deployment device with a sampling end-effector touches the surface and acquires sample in a short-duration transient operation i.e. touch-and-go sampling. This is followed by a departure from the close proximity once the touch-and-go operation has been determined to have completed.

Previous analysis at JPL has considered the deployment and retrieval of the end-effector, anchoring, or in-situ sampling device by means of a multi-link or continuous manipulator. Different sampling arm types that have been considered inclide: a) a rigid, multi-link articulated arm with joint control; b) a flexible deployable, coilable boom with locking joints; c) a deployable truss with joint control; and d) a continuum boom with distributed control. Figure 15 shows the components included in the system level multibody dynamics analysis model of spacecraft, manipulator, and small body. Figure 16 shows snapshots from the simulation of distributed control of continuous deployable boom interacting with the surface.[15,16,17]

G. Surface Anchoring

Activities such as drilling or coring on the surface of the NEO will require **Anchored Operations**. The performance of the anchor in terms of its deployment into the NEO regolith, the holding strength of the anchor, and its retrieval requires consideration of the geometry-dependent force iteration with the large number of particles constituting the "rubble" and other material that make up the NEO. In the low-gravity environment, cohesion forces can play an important role in addition to frictional forces.

Effective NEO exploration requires vehicle/astronaut anchoring due to extremely low gravity. Simulation and testing must be carried out with implications on system/mission design, system V&V, design of combined vehicle/human/robot teams, design of proximity operations such as: landing, tethered operations, surface mobility, drilling, sub-surface sampling. EVA requires innovative tethering/anchoring techniques for the

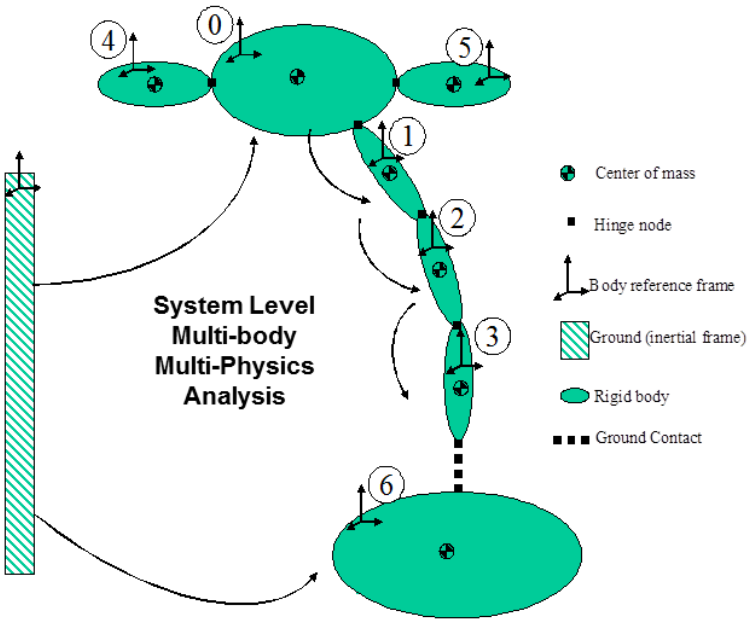

Figure 15. System level multibody dynamics analysis model of spacecraft, manipulator, and small body

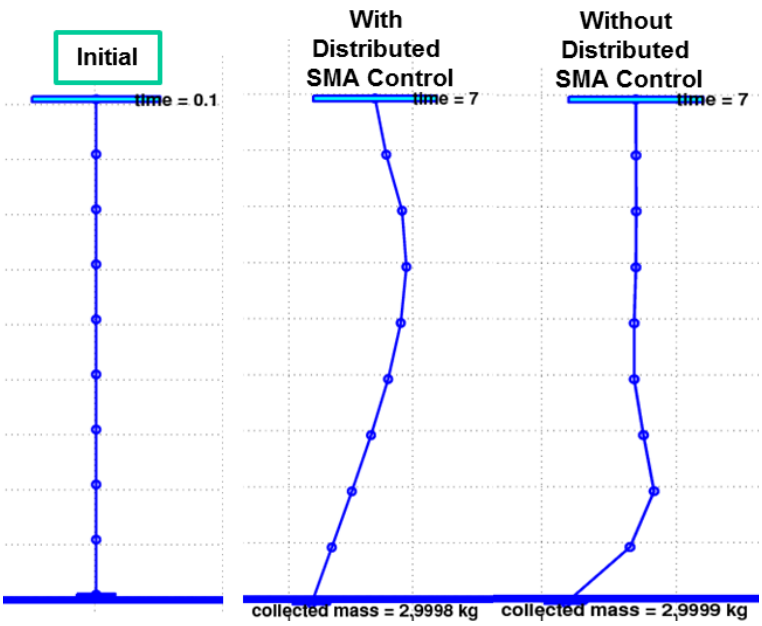

Figure 16. Snapshots of simulation of distributed control of continuous deployable boom interacting with surface

astronauts to move in the vicinity of a Small Body. In all these cases, a motorized winch network may provide support for astronaut surface operations. A motorized winched network also provides the vertical reaction force needed for drilling and sample collection. Robot arm sampling device interactions with terrain during sample collection need to be understood. Hopping/crawling robots may interact with regolith material on surface of NEO and can hop at various angles with adjustable strengths to achieve a desired vertical height or horizontal distances. Anchors may be used as hand or footholds, or possible attach points for ropes that hold an astronaut or equipment to the surface. Figure 17 depicts three types of anchors interacting with regolith simulant.

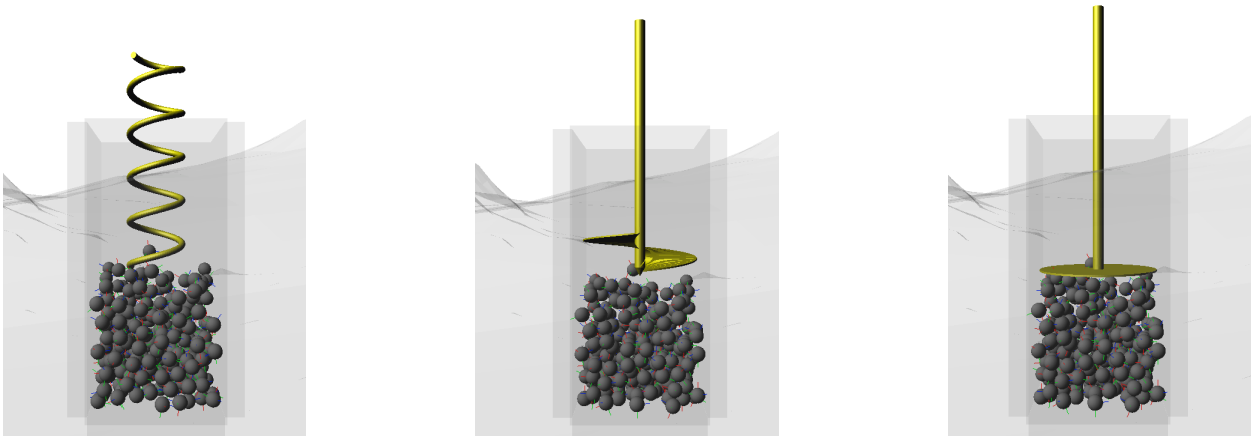

(a) Spiral Anchor (b) Helical Anchor (c) Disc Anchor

Figure 17. Three types of anchors interacting with regolith simulant.

Present understanding is that all asteroids that have been observed at close range appear to be covered by meters of strength-less regolith, in which case the anchor pull-out capacity is dependent on the weight of the overlying material. Large asteroidal bodies typically spin slowly and may have more strength-less material on the surface than small bodies, which tend to spin faster. This understanding implies that, in general, slow anchoring methods such as those based on drilling or melters will require the spacecraft ACS to be involved for vehicle stabilization. Conversely, fast anchoring method such as those based on tethered spikes, telescoping spikes, and multi-legged with tethered or telescoping spikes will likely require less ACS involvement. Early studies on anchoring for the ST4/Champollion mission selected a 1 kg 1.9cm diameter truncated cone penetrator for anchoring onto the surface on materials of strength up to 10 Mpa with a 45 degree impact angle within a reasonable velocity range (100-200 m/s) with a minimum pullout resistance of 450 N in any direction.

Several anchoring deployment/retrieval issues must be carefully considered that can impact the mission design. An anchor may ricochet adversely on surface instead of solidly emplacing on ground. Also, drilling a helical anchor requires a torque transfer to another object. PHILAEs landing gear uses ice screws and three landing legs with two pods in each, for example. Harpoons can be easily launched before landing. More than one anchor needs to be deployed from the spacecraft to ensure static stability. Spacecraft ACS (reaction wheels, not RCS) will probably need to be on during the Anchoring Phase to avoid slack cables and vehicle stability problems. Some anchor designs will allow them to be pulled out, others will not. Figure 18 shows results from a simulation of anchor penetration in a granular media, with typical acceleration response of the anchor during penetration.

V. Conclusion

We have described a end-to-end, physics-based modeling, analysis and simulation capability developed at JPL for NEO missions. The developed SEAS tool leverages highly validated spacecraft and mission simulation software at JPL. Important extensions to model NEO regolith are in progress, and a number of analysis scenarios have been described. This tool provides a comprehensive systems engineering capability to answer key questions, validate requirements, conduct key system and mission trades, and evaluate performance and risk related to NEO operations for any proposed human or robotic missions to a NEO.

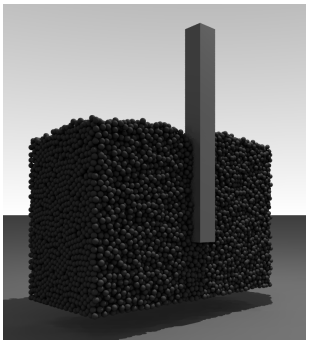

(a) Granular Media

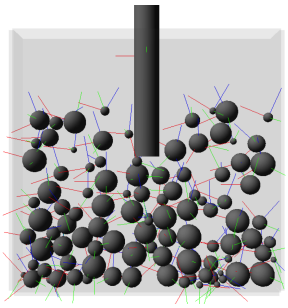

(b) Instrumented Media

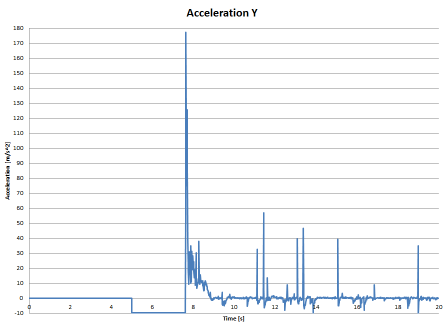

(c) Force Profiles

Figure 18. Simulation of anchors penetrating a granular media.

VI. Acknowledgment

This work was carried out at the Jet Propulsion Laboratory, California Institute of Technology, under a contract with the National Aeronautics and Space Administration. We thank our NASA Program Manager, Doug Craig, our JPL Program Manager, Steve Wall, and our collaborators at the NASA Langley Research Center, NASA Johnson Space Center, and Jet Propulsion Laboratory for support in the development of SEAS. We also wish to thank our collaborators at NASA JSC for the collaborations leading to the enhancement of the Dshell/DSENDS framework. The JPL Research and Technology Development (RTD) fund is acknowledged for supporting some of the analysis work related to NEO operations. The research conducted by R Patton was carried out at the Jet Propulsion Laboratory, California Insti- tute of Technology, and was sponsored by the Undergraduate Student Research Program and the National Aeronautics and Space Administration. The research conducted by H. Kline was carried out at the Jet Propulsion Laboratory, California Institute of Technology, and was sponsored by the Summer Internship Research Program and the National Aeronautics and Space Administration. The research conducted by H. Mazhar was carried out at the Jet Propulsion Laboratory, California Institute of Technology, and was sponsored by the SEAS task at the University of Wisconsin under a contract with JPL and the National Aeronautics and Space Administration. The authors would also like to thank T. Medford and D. Melanz for their contributions to this work.

References

[1]Jain, A., Cameron, J., Lim, C., and Guineau, J., "SimScape Terrain Modeling Toolkit," *Second International Conference on Space Mission Challenges for Information Technology (SMC-IT 2006)*, Pasadena, CA, July 2006.

[2]Pomerantz, M., Jain, A., and Myint, S., "Dspace: Real-time Visualization System for Spacecraft Dynamics Simulation," *Proceedings of the Third IEEE International Conference on Space Mission Challenges for Information Technology (SMC-IT 2009), Pasadena, CA*, July 2009.

[3]Nayar, H., Balaram, J., Cameron, J., Jain, A., Lim, C., Mukherjee, R., Peters, S., Pomerantz, M., Reder, L., Shakkottai, and Wall, S., "A Lunar Surface Operations Simulator, Proceedings of the Simulation, Modeling, and Programming for Autonomous Robots," *SIMPAR 2008*, Venice, Italy, Nov. 2008, pp. 65–74.

[4]Nayar, H., Balaram, J., Cameron, J., Lim, C., Mukherjee, R., Pomerantz, M., Reder, L., Myint, S. Serrano, N., and Wall, S., "Recent Developments on a Simulator for Lunar Surface Operations," *Proceedings of the AIAA SpaceOps Conference 2009*, AIAA, Pasadena, CA, Sept. 2009.

[5]Nayar, H., Balaram, J., Cameron, J., DiCicco, M., Howard, T., Jain, A., Kuwata, Y., Lim, C., Mukherjee, R., Myint, S., Palkovic, A., Pomerantz, M., and Wall, S., "Surface Operational Analyses for Lunar Missions," .

[6]Jain, A. and Man, G., "Real–Time Simulation of the Cassini Spacecraft Using DARTS: Functional Capabilities and the Spatial Algebra Algorithm," *5th Annual Conference on Aerospace Computational Control*, Aug. 1992.

[7]Biesiadecki, J., Henriquez, D., and Jain, A., "A Reusable, Real-Time Spacecraft Dynamics Simulator," *16th Digital Avionics Systems Conference*, Irivine, CA, Oct. 1997.

[8]Jain, A., Guineau, J., Lim, C., Lincoln, W., Pomerantz, M., Sohl, G., and Steele, R., "Roams: Planetary Surface Rover Simulation Environment," *International Symposium on Artificial Intelligence, Robotics and Automation in Space (i-SAIRAS 2003)*, Nara, Japan, May 2003.

[9]Jain, A., Balaram, J., Cameron, J., Guineau, J., Lim, C., Pomerantz, M., and Sohl, G., "Recent Developments in the ROAMS Planetary Rover Simulation Environment," *IEEE 2004 Aerospace Conf.*, Big Sky, Montana, March 2004.

[10]Balaram, J., Austin, R., Banerjee, P., Bentley, T., Henriquez, D., Martin, B., McMahon, E., and Sohl, G., "DSENDS

- A High-Fidelity Dynamics and Spacecraft Simulator for Entry, Descent and Surface Landing," *IEEE Aerospace Conference*, Big Sky, Montana, March 2002.

[11]Scheeres, D., Hartzell, C., Sanchez, P., and Swift, M., "Scaling forces to asteroid surfaces: The role of cohesion," *Icarus*, Vol. 210, 2010, pp. 968–984.

[12]Biele, J., Ulamec, S., Richter, L., Khrt, E., Knollenberg, J., and Mhlmann, D., "The Strength of Cometary Surface Material: Relevance of Deep Impact Results for Philae Landing on a Comet," *Deep Impact as a World Observatory Event: Synergies in Space, Time, and Wavelength*, edited by H. Kufl and C. Sterken, Vol. 45 of *ESO Astrophysics Symposia*, Springer Berlin / Heidelberg, 2009, pp. 285–300.

[13]Biele, J. and et al., "The putative mechanical strength of comet surface material applied to landing on a comet," *Acta Astronautica*, Vol. 65, 2009, pp. 11681178.

[14]Komle, N. and et al., "Impact penetrometry on a comet nucleus interpretation of laboratory data using penetration models," *Planetary and Space Science*, Vol. 49, 2001, pp. 575598.

[15]Quadrelli, B., Backes, P., Wilkie, W., Keim, J., Quijano, U., Mukherjee, R., Scharf, D., Bradford, S., and McKee, M., "Investigation of Phase Transition-Based Tethered Systems for Small Body Sample Capture," *Acta Astronautica*, Vol. 68, 2011, pp. 947–973.

[16]Quadrelli, B., Backes, P., Wilkie, W., Keim, J., and Quijano, "Modeling and Testing of Phase Transition-Based Deployable Systems for Small Body Sample Capture," *17th AIAA/ASME/AHS Adaptive Structures Conference*, Palm Springs, California, May 2009.

[17]Quadrelli, B., Backes, P., Wilkie, W., Keim, J., and Quijano, "Deployable Tethered Systems for Planetary Sample Capture," .